2025 American Control Conference (ACC)
July 8-10, 2025. Denver, CO, USA

Control of an UAV swarm in amorphous formation

Benjamin Piet
Guidage Navigation Contrôle (GNC)
Institut Saint Louis (ISL)
Saint-Louis, France
benjamin.piet@isl.eu

Guillaume Strub, Sébastien Changey
Guidage Navigation Contrôle (GNC)
Institut Saint Louis (ISL)
Saint-Louis, France
{guillaume.strub,sebastien.changey}@isl.eu

Nicolas Petit
Centre Automatique Système (CAS)
Mines Paris, PSL University
Paris, France
nicolas.petit@minesparis.psl.eu

***Abstract*—Formation flying, particularly in swarms, has become a prominent area of interest for UAV applications. While rigid formation shapes offer several advantages, they also increase the likelihood of detection by optical or radar systems. Drawing inspiration from materials science and condensed matter physics, this paper proposes a method to provide to a formation an amorphous appearance, thereby reducing the swarm's detectability. The proposed technique involves the introduction of a virtual obstacle that performs stochastic movements within the formation. Two simple metrics are introduced to evaluate the effectiveness of this approach: one assesses the formation's resemblance to a rigid body, while the other measures the internal velocity correlation among the UAVs. Simulation results validate the effectiveness of this method.**

***Index Terms*—Autonomous systems, Multivehicle systems, Cooperative control**

I. Introduction

The subject of coordinated flight for swarms of unmanned aerial vehicles (UAVs, a.k.a. drones) has received significant interest in recent decades, both for civilian applications such as search and rescue, mobile sensor networks, and large-scale transportation, as well as for military purposes including surveillance, reconnaissance, and combat missions.

A common goal in these applications can be described as guiding the swarm to a designated target while preventing collisions with both the environment and other swarm members. To accomplish this, it is often recommended that the UAVs fly in a specific formation to optimize aerodynamic efficiency, defense saturation, intelligence-gathering capabilities, or firepower concentration in the case of armed aerial vehicles.

Multiple techniques are available for formation control and obstacle avoidance in UAV swarms. For example, virtual structure [1], [2], consensus-based strategies [3], or even Model Predictive Control [4], [5] are often considered for formation keeping, see also [6], [7]. This article considers a method based on artificial potential fields from [2], with additional repulsive and rotational potential fields to avoid obstacles [8]–[10].

Despite all the beneficial aspects, formation flight can also appear as a drawback in a military context. Indeed, keeping a strict formation makes the swarm much easier to detect. While UAVs are usually highly maneuverable vehicles, a formation is, by definition, a rigid and slow maneuvering structure, relatively easy to track with optical or radar technologies [11]–[14].

The paper therefore proposes a solution to make the swarm less prone to detection. Taking inspiration from the field of material sciences, we introduce the notion of amorphousness which, in the case of material science refers to the characteristic of a material in which elements are "bound in disordered, random spatial positions" [15]–[17]. This definition is here adapted to the case of UAV swarms, and implemented by introducing a virtual obstacle (referred to as the "disruptor") within the swarm, producing slicing and strains in the rigid formation. Its effect on the formation is illustrated in Fig. 1.

The paper is organized as follows : given the notation and the control technique used for formation flight and obstacle avoidance in Section II, we present in Section III the proposed method to disturb the formation. Then, in Section IV, we present simulation results, with the introduction of two metrics, one assessing the similarity to a rigid formation and the other evaluating velocity correlations within the swarm. We finally conclude this paper with the a discussion over the limitations of our approach and perspectives of improvement.

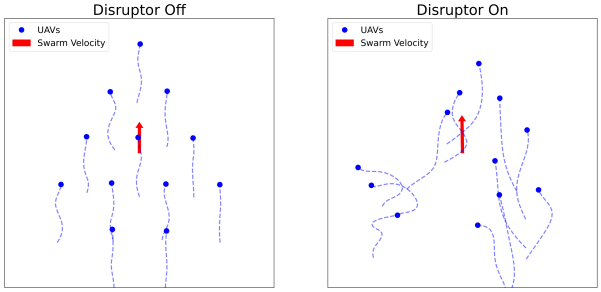

Fig. 1. Effect of the disruptor method. Close-up views of the swarm from a mobile reference frame centered on its barycenter, along with the group velocity (red arrow). (Left) The swarm moves smoothly toward its target (not shown) after successfully avoiding obstacles, with the arrow-shaped formation clearly visible. (Right) The UAVs are still heading towards the target, but the formation shape becomes difficult to discern due to the disruptor freely moving within the swarm.

979-8-3315-6937-2/$31.00 ©2025 AACC

II. UAV SWARM MODEL AND CONTROL

A. Notations

A homogeneous swarm of N UAVs is considered. Note $\mathbf{q}_i = [x_i, y_i]^T \in \mathbb{R}^2$ the position of each UAV $i = 1, ..., N$ w.r.t. a fixed global planar reference frame. The Euclidean norm is noted $||.||$ and $\langle \cdot\ ,\ \cdot \rangle$ is the scalar product.

It is desired that the swarm flies in a formation defined by the collection of vectors (matrix)

$$\mathbf{l} = (\mathbf{l}_{12}, ..., \mathbf{l}_{N-1,N}) \tag{1}$$

with $\mathbf{l}_{ij} = \mathbf{q}_i - \mathbf{q}_j$, $i, j = 1, ..., N$. Each edge in the formation shall be occupied by one (and only one) UAV. This vector unambiguously defines the formation and the relative positions of the UAVs.

The flight area contains N_{obs} obstacles, having known locations $\mathbf{q}_k^{obs} = [x_k^{obs}, y_k^{obs}]^T \in \mathbb{R}^2$ for $k = 1, ..., N_{\text{obs}}$.

B. Formation control and obstacle avoidance

Each UAV is assumed to follow ideal first-order dynamics

$$\dot{\mathbf{q}}_i = \mathbf{u}_i \quad \forall i \in (1, ..., N) \tag{2}$$

with $\mathbf{u}_i$ being the commanded velocity vector. The value of $\mathbf{u}_i$ is chosen to satisfy three control objectives.

First, it is desired that the UAVs align their velocity with a particular vector $\mathbf{u}_d$. For this purpose a global swarm velocity vector is defined using the vector between the position of the goal $\mathbf{q}^{goal}$ and the barycenter of the swarm (with $k_a > 0$)

$$\mathbf{u}_d = k_a(\mathbf{q}^{goal} - \frac{1}{N}\sum_{i=1}^{N} \mathbf{q}_i)$$

Second, for keeping the specified formation shape a local potential function is used (see [2]). And third, for obstacle avoidance, repulsive and rotational repulsive forces around the obstacles are added to the velocity command $\mathbf{u_i}$ sent to the UAV [9]. Combining the above ingredients yields

$$\mathbf{u}_i = \mathbf{u}_d - \mathbf{C}\sum_{j \neq i} \mathbf{\Phi_{ij}} + \sum_{k}^{N_{\text{obs}}} \mathbf{F}_{i,k}^{rep} + \sum_{k}^{N_{\text{obs}}} \mathbf{F}_{i,k}^{rot} \tag{3}$$

where each term respectively corresponds to the global swarm velocity command, the formation potential function, the repulsive and the rotational repulsive forces. In the above, $\mathbf{C}$ is a symmetric positive definite matrix, and

$$\mathbf{\Phi_{ij}} = \mathbf{q}_i - \mathbf{q}_j - \mathbf{l}_{ij} + \delta\gamma(\frac{1}{\beta_{ijl}^{2\gamma}} - \beta_{ij}^{2\gamma})\beta_{ij}^{\gamma-1}(\mathbf{q}_i - \mathbf{q}_j)$$

with $\beta_{ij} = \frac{1}{2}\|\mathbf{q}_i - \mathbf{q}_j\|^2$, $\beta_{ijl} = \frac{1}{2}\|\mathbf{l}_{ij}\|^2$, δ and γ two positive parameters to select.

The repulsive forces created by the N^{obs} obstacles on the i^{th} UAV is the sum of all the forces $\mathbf{F}_{i,k}^{rep}$ created by each obstacle k on the i^{th} UAV. Noting the logic statement $A = (||\mathbf{q}_i - \mathbf{q}_k^{obs}|| < d_0)$, one has

$$\mathbf{F}_{i,k}^{rep} = \begin{cases} k_r(\frac{1}{||\mathbf{q}_i - \mathbf{q}_k^{obs}||} - \frac{1}{d_0})\frac{1}{||\mathbf{q}_i - \mathbf{q}_k^{obs}||^2}\mathbf{OD}_i^k & \text{if } A \text{ is true,} \\ 0 & \text{otherwise} \end{cases}$$

with $\mathbf{OD}_i^k$ the unit vector from the obstacle k to the UAV i, $k_r > 0$ and $d_0 > 0$ the radius of influence of the obstacle (tuning parameters).

Finally, the rotational forces (see [8], [9])

$$\mathbf{F}_{i,k}^{rot} = k_g \begin{bmatrix} 0 & -\omega_{i,k} \\ \omega_{i,k} & 0 \end{bmatrix} \mathbf{OD}_i^j$$

with $k_g > 0$, and $\omega_{i,k}$ calculated as

$$\omega_{i,k} = \begin{cases} \frac{1}{\|\mathbf{q}_i^{obs} - \mathbf{q}_i)\|} & \text{if } A \wedge B \text{ is true} \\ \frac{-1}{\|\mathbf{q}_k^{obs} - \mathbf{q}_i\|} & \text{if } A \wedge \neg B \text{ is true} \\ 0 & \text{if } \neg A \text{ is true} \end{cases}$$

where $B = (\det[\mathbf{q}_k^{obs} - \mathbf{q}_i, \mathbf{q}^{goal} - \mathbf{q}_i] \geq 0)$.

The control law of Eq. (4) has been experimentally tested in the context of a confined environment. It possesses the desirable properties of reaching the goal (asymptotically, even if the goal is moving) without collision between the UAVs, or with obstacles, as expected from the theoretical works of [2], [8]–[10], even in the presence of communication delays and computational lags due to fast reconfiguration by optimization-based techniques. For a detailed account of these experiments conducted on a Crazyflie[1]-based platform, refer to [18].

III. DISTURBING A SWARM

A. Amorphousness

The main idea of the paper is to disturb the swarm's formation to give its internal structure the property of amorphousness.

Amorphousness is a concept from condensed matter physics and material science. It refers to the characteristic of a material in which the atoms, unlike in a crystalline state, are "bound in disordered, random spatial positions" [15], with "no long-range periodicity" [16], no lattice periodicity, nor any translational invariance or symmetry in tiling [17].
Amorphousness, which is related to the notion of complexity, should not be mistaken for randomness (see [19]). Randomly perturbing individual positions with noise does not suffice to create amorphousness because, unless very large random offsets are used, the spatial correlations mentioned above persist. Amorphousness can be mathematically described in the theory of computational mechanics [19], using hidden Markov models, or through information theory, e.g., via Shannon's entropy, universal Turing machines, and Kolmogorov-Chaitin (KC) complexity [20].

Being amorphous has an impact on the detectability of UAVs. Two main classes of technology are commonly used to detect flying objects: vision and radar (see [11]–[13], [21], [22]). Visual detection of a UAV swarm becomes more challenging when the movements of individual UAVs are not clearly correlated. Additionally, it is harder to determine the swarm's target if it is unclear that the UAVs are flying as a coordinated group.

[1]See at https://www.bitcraze.io/products/crazyflie-2-1/

Though no clear study has been published on the subject yet, radar detection is also likely to be troubled by amorphousness. This is discussed next.

In the case of a crystalline material, illuminating the structure with radio frequency waves (typically X-rays) will result in constructive and destructive interferences giving birth to diffraction patterns [23]. These patterns, taking the shape of peaks in the diffraction diagram (Bragg's peaks), are not visible in the case of an amorphous material (which produce diffuse scattering instead of interferences). With well tailored wave length (of the order of magnitude as the distance between UAVs, e.g. decimeter band wave lengths (UHD, S-Band, L-Band...)[2], the same type of phenomenon should be witnessed in the case of a UAV formation being observed with a radar [26].

In the context of UAV swarms, we quantify amorphousness using two metrics depending on q_i, and $\dot{q}_i$, that mainly relate to the capability of an external observer to not discern a rigid shape structure inside the swarm. The structure should avoid spatial, but also temporal patterns, as to make it harder to identify any kind of rigidity.

Our current method, using Eq. (4), is made to keep the UAVs as much as possible in the formation shape defined by the vector $\mathbf{l}$ (see Eq. (1)). Our goal then is to add a corrective term to this control to provide the desired amorphousness. This can be summed up with the following:

Main problem. *Given Eqs.* (2) *and* (3)*, find an additional term in* (3) *that provides amorphousness to the swarm.*

B. Introducing a disruptor

To create the desired amorphousness, we propose a novel approach that introduces a virtual obstacle (later on referred to as *disruptor*)[3] confined within the formation's boundaries. The rationale is that the virtual obstacle will force movement inside the formation, creating clusters of different densities, at various spots of the formation at each collision. Making this obstacle move in a random pattern will avoid repetitive motion of the disruptor. It behaves much like *ball milling*, an established technique employed to produce amorphous materials through blending and grinding of substances like minerals, compounds, alloys, or ice crystals [27].
With the added disrupting obstacle, the velocity command of each UAV Eq. (3) becomes

$$\mathbf{u}_i = \mathbf{u}_d - \mathbf{C}\sum_{j\neq i}\mathbf{\Phi}_{ij} + \sum_{k}^{N_{obs}+1}\mathbf{F}_{i,k}^{rep} + \sum_{k}^{N_{obs}+1}\mathbf{F}_{i,k}^{rot} \quad (4)$$

The disruptor is a circular obstacle of radius r^d. Note $\mathbf{q}^d$ its position, and $\mathbf{v}^d$ its velocity.

[2]Many studies report usage of (multi-static) radars operating in S-band (2.4 GHz) to exploit the Micro-Doppler signatures (mDS) generated by the fast rotation of the UAVs blades, see e.g. [24] where coherent pulses are employed, and [25] for radar signatures classification and references therein for experimental validation using X-band (9.7 GHz) radars.

[3]The idea can be extended to multiple disruptor.

Note $\mathbf{q}^s$ the barycenter of the positions of all the UAVs, and $\mathbf{v}^s$ its velocity.

$$\mathbf{q}^s = \frac{1}{N}\sum_i \mathbf{q}_i, \quad \mathbf{v}^s = \dot{\mathbf{q}}^s$$

The disruptor is freely moving inside a disc centered at $\mathbf{q}^s$ with a fixed radius r^s, chosen to cover the formation defined by (1). When the disruptor reaches the boundary of the disc it "bounces" in a new direction as illustrated on Fig. 2. We note $\alpha_n \in [-\frac{\pi}{2}, \frac{\pi}{2}]$ the angle defining the new direction (for the n^{th} bounce) of the disruptor and at each bounce, its velocity vector $\mathbf{v}^d$ is updated following

$$\mathbf{v}^d = \mathbf{v}^s + \mathbf{v}^d_{rel} = \mathbf{v}^s + V\, R_{\alpha_n}\frac{\mathbf{q}^s - \mathbf{q}^d}{\|\mathbf{q}^s - \mathbf{q}^d\|}$$

where R_{α_n} is the rotation matrix of angle α_n in the plane, and $V > 0$. Similarly to a sweeping process [28], $\mathbf{v}^d$ remains constant within the fixed reference frame until the disruptor touches the formation circular enclosure and gets its velocity updated again according to Section III-B.

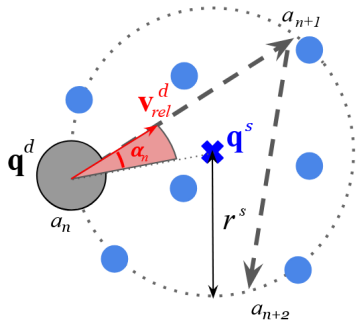

Fig. 2. The disruptor bounces within the formation circular enclosure.

C. Nature and amplitude of the bouncing angle

1) Avoiding cycles: Under some circumstances, the motion of the disruptor may be periodic, which is not desirable. Consider the case when $\mathbf{v}^s$ is a constant vector, which is often the case during long distance flight. Noting $(a_n)_{n\in\mathbb{N}}$ the arguments of the impact points on the circular enclosure and $(\alpha_n)_{n\in\mathbb{N}}$ the sequence of (incidence) angles between the outgoing velocity and the radius of impact, the recurrence equation is

$$a_{n+1} = a_n + 2\alpha_n - \text{sign}(\alpha_n)\pi$$

If the bouncing angle is chosen constant, i.e. $\forall n \in \mathbb{N},\ \alpha_n = \alpha$, then the relation becomes $a_n = a_0 - n(\pi - 2\alpha)$ with a_0 the initial argument. This relation generates a cyclic sequence on the unit circle if and only if there exists $(q, p) \in \mathbb{Z}$ s.t. $-p(\pi - 2\alpha) = 2\pi q$ i.e.

$$\alpha = \pi(\frac{1}{2} + \frac{q}{p}) \quad (5)$$

In this case, p will be the length of the cycle, and q the winding number of the disruptor w.r.t. $\mathbf{q}^s$. To avoid these cycles, it is necessary to avoid the values in the set (5), i.e.

the rational multiples of π. The solutions to this issue is to either select a constant α that does not satisfy the cycle condition, or to introduce randomness in the choice of the bouncing angle.

2) Optimizing area coverage: It is desired that within a few bounces, the disruptor covers a vast percentage of the formation surface. This gives it more chances to create amorphousness everywhere in the formation over a given observation period. The area covered by the disruptor (having r^d as radius) can be numerically determined[4]. In the general case, no analytic solution can be easily found. Fig. 3 shows for instance the coverage pattern of the disruptor in the case of a constant bouncing angle over 12 bounces.

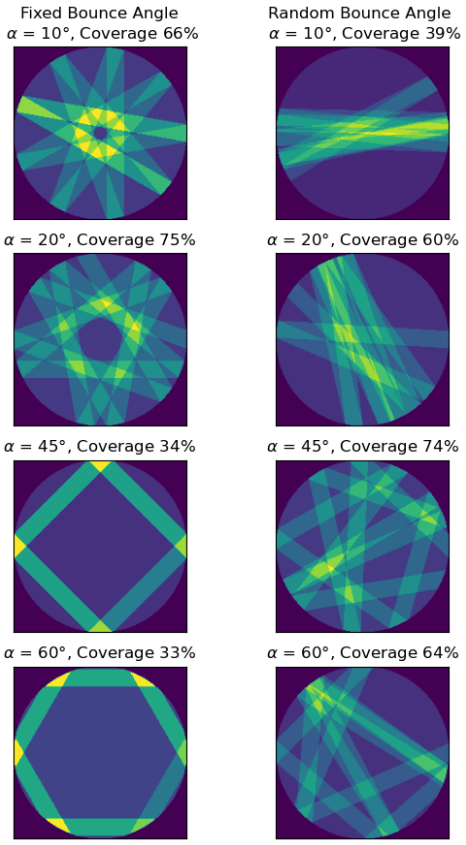

Fig. 3. Coverage pattern of the disruptor and coverage percentage of the enclosing circle, with $r^d = \frac{1}{10}r^s$, and limited to 12 bounces. At each bounce, the new bounce angle is either fixed and deterministic (left), or taken from a uniform distribution over $[-\alpha, \alpha]$ (right). Yellow zones are zones of most frequent presence of the disruptor.

This evaluation allows comparing between taking a fixed α_n or taking a random angle at each bounce. Fig. 4 reports the coverage obtained in a limited number of bounces (6 and 12 here) for different angle values, corresponding to the constant bouncing angle in the case of a fixed α_n, and corresponding to the amplitude of the uniform distribution of the choice of α_n in the case of a random bouncing angle.

For a fixed angle, the coverage seems to be better around low values of α (typically for α between 10^o and 20^o), and

[4]For this purpose a mesh is defined on the disc, and the occurrences of presence of the disruptor are counted for each cell of the mesh.

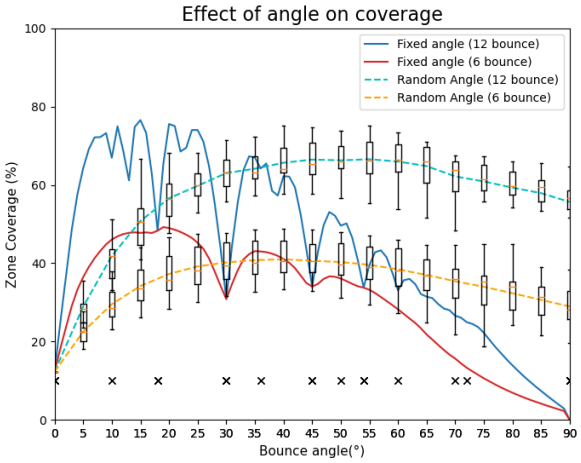

Fig. 4. Comparisons of coverage percentage for fixed and random bounce angle, for a total of 6 and 12 bounces, and a disruptor radius $r^d = \frac{1}{10}r^s$. The bounce angle α_n is either constant of value α, or uniformly randomly distributed over $[-\alpha, \alpha]$.

it decreases when α increases. Also we notice some drops in terms of coverage for some specific values of α in case of a fixed angle. Indeed these drops are expected from the previous discussion in Section III-C1. The black crosses on the figure correspond to values of α that satisfy Eq. (5) for $p < 12$ (cycle shorter than number of bounces), and it can be easily checked that the drops in coverage correspond to values of α that create short cycles (for instance $\alpha = 30^o$ corresponds to $q = -1$ and $p = 3$). Interestingly, we see that random selection of bouncing angles provides higher and more uniform coverage rates from 30^o to 60^o. Given that random angles will not create any cycles, this represents a valuable choice.

Another point of interest is the distribution of the bouncing points on the circle. The sequence (a_n) can be readily studied. A straightforward calculus yields $a_{n+2} = a_n + 2\alpha_n + 2\alpha_{n+1} \mod 2\pi$ and, thus one can easily obtain, for all $n \geq 1$,

$$a_{2n-1} = a_0 - \text{sign}(\alpha_0)\pi + \sum_{i=0}^{2n-2} 2\alpha_i \mod 2\pi \quad (6)$$

$$a_{2n} = a_0 + \sum_{i=0}^{2n-1} 2\alpha_i \mod 2\pi \quad (7)$$

The α_i are *independent* random variables, with uniform distributions on $[-\alpha, \alpha]$. So as $n \to \infty$, the distributions of a_{2n} and a_{2n+1} will converge to a Gaussian according to the central limit theorem [29], for which we can easily calculate the mean and standard deviation. The distribution shape of a_{2n} and a_{2n+1} will depend on the amplitude α, but also on the number of bounces. As n increases, the two distributions take more and more the shape of a Gaussian, getting gradually flatter. So for n high enough and for a chosen amplitude, we can guarantee that every point on the circle can be visited (from a stochastic point of view). The higher the amplitude, the lower n can be to have this guarantee.

D. Tuning the parameters

The disruptor method we propose is defined by a list of parameters that can be gathered into 3 groups: *i*) the parameters that are related to the mission, and are thus fixed like the number of UAVs N, the radius r^s of the formation, and the velocity of the swarm $\mathbf{v}^s$, *ii*) the parameters that act on the control of the UAVs, that have been fine-tuned in the process described in [18] (see Section IV-A for the values), *iii*) finally the parameters linked to the bouncing of the disruptor, that still need to be chosen: nature and amplitude α of the bouncing angle α_n, the velocity V and the radius r^d of the disruptor

For the bouncing angle sequence α_n, we have seen earlier that choosing a random sequence yielded overall good results in terms of coverage compared to a constant bouncing angle, and had the advantage of not creating any cycle. For the amplitude α, the best results were obtained for $\alpha \in [30^o, 60^o]$, so following further tests the middle of the range $\alpha = 45^o$ was chosen. We then chose to have the disruptor bounce in the disc approximately every 2 seconds, so noting T this period gives us the relative velocity $V = 2r^s/T$. Finally, we have chosen the disruptor dimension such that each bounce covers between a third and half of the disc. This led us to choose $r^d = \frac{r^s}{2}$ after some testing. These two last parameters have of course a great impact the quality of the amorphous aspect we are aiming for. Making it bounce too slow will have just give a deformed static formation shape, while making it too fast wont give enough time for teh UAVs to try and avoid the obstacle. The same logic can be applied for the size of the disruptor, where too small wont have any effect, and too big will push the UAVs in blocks. Tuning these two parameters was done with testing in simulation, to try and find this "goldylock" area.

IV. Simulation Results

In this section we present the results from simulations, with first some plots to show the effectiveness and practicality of our control method, then in a second part we introduce two metrics to quantify the amorphousness of the swarm.

A. Parameters Values

Table I reports the values used for the control parameters.

TABLE I
VALUES OF TUNING PARAMETERS FOR CONTROL.

k_a (-)	γ (-)	δ (-)	c (-)	k_r (-)	k_g (-)	d_0 (m)	d (m)
0.2	1	0.002	0.2	0.02	0.1	1	0.6

With $\mathbf{C} = c\mathbf{I}$ and d the minimal value of $||\mathbf{l}_{ij}||$. Furthermore, the velocity of each UAV is bounded by $V_{max} = 1$ m/s. The disruptor parameters values are given in Table II.

B. Effect of the disruptor, formation control and obstacle avoidance

A handy feature of the proposed disruptor method, is that it can be activated or de-activated at the flick of a switch, by simply considering or removing the disruptor from the list of obstacles in Eq. (4).

TABLE II
VALUES OF TUNING PARAMETERS FOR THE DISRUPTOR.

r^s (m)	r^d (m)	α (°)	V (m/s)
2	1	45 (random)	1

To illustrate this, the scenario at hand consists of a small swarm of 12 UAVs, tasked with reaching two goals in the zone in a certain order, while keeping an arrow-like formation. They encounter an obstacle on the way to the first objective, and no disruptor is active. On the way to the second objective, the obstacle is not met (it is too far on the left of the formation), but the disruptor is activated.

As shown on Fig. 5, the UAVs pass around the obstacles without any issue or collisions, and keep as much as possible the arrow shape (while allowing some changes to it to avoid rigidity).

Then, on the second part of the demonstration on Fig. 5, where the disruptor is activated, one can clearly see that the swarm does not keep its arrow shape, and that the UAVs move in an amorphous manner.

C. Quantifying amorphousness

Below, we present two metrics that can be used to quantify the amorphousness of the swarm.

The first metric aims at measuring how well a group movement can be identified from the movement of the swarm. The idea is to try fitting the behavior of a rigid virtual structure to the observed swarm movement.

In a rigid virtual structure with N nodes, the velocity of the node i, written v_i can be expressed as

$$\mathbf{v}_i = \mathbf{v}^s + \mathbf{\Omega} \times \mathbf{l}_i$$

with $\mathbf{v}^s$ the velocity of the swarm, $\mathbf{\Omega}$ the rotation velocity vector of the formation, and $\mathbf{l}_i = \mathbf{q}_i - \mathbf{q}^s$. So we can write it as

$$\mathbf{v}_i = A_i(t) \begin{bmatrix} \mathbf{v}^s \\ \mathbf{\Omega} \end{bmatrix} \triangleq \begin{bmatrix} I & [\mathbf{l}_i(t)]_\times \end{bmatrix} \begin{bmatrix} \mathbf{v}^s \\ \mathbf{\Omega} \end{bmatrix} \tag{8}$$

where $[.]_\times$ is the skew-symmetric matrix associated to the cross product with its argument, ie the matrix that when doing standard matrix multiplication with a vector has the same effect as the cross product with the vector associated to the matrix.

Noting $\mathbf{v}(t) \triangleq [\mathbf{v}_1(t)^T, ..., \mathbf{v}_N(t)^T]^T$ and $A(t) \triangleq [A_1(t)^T, ..., A_N(t)^T]^T$, we obtain a classic linear regression problem $\mathbf{v}(t) = A(t) \begin{bmatrix} \mathbf{v}^s \\ \mathbf{\Omega} \end{bmatrix}$, with $\mathbf{v}^s$ and $\mathbf{\Omega}$ the two unknown variables to be found. This serves to define the following performance index.

Performance index 1 (stress and torsional flexibility)**.** *The* stress flexibility *of the velocities $v(t)$, respectively the* torsional flexibility*, is defined as $\sigma_v(t)$ and $\sigma_\Omega(t)$ where*

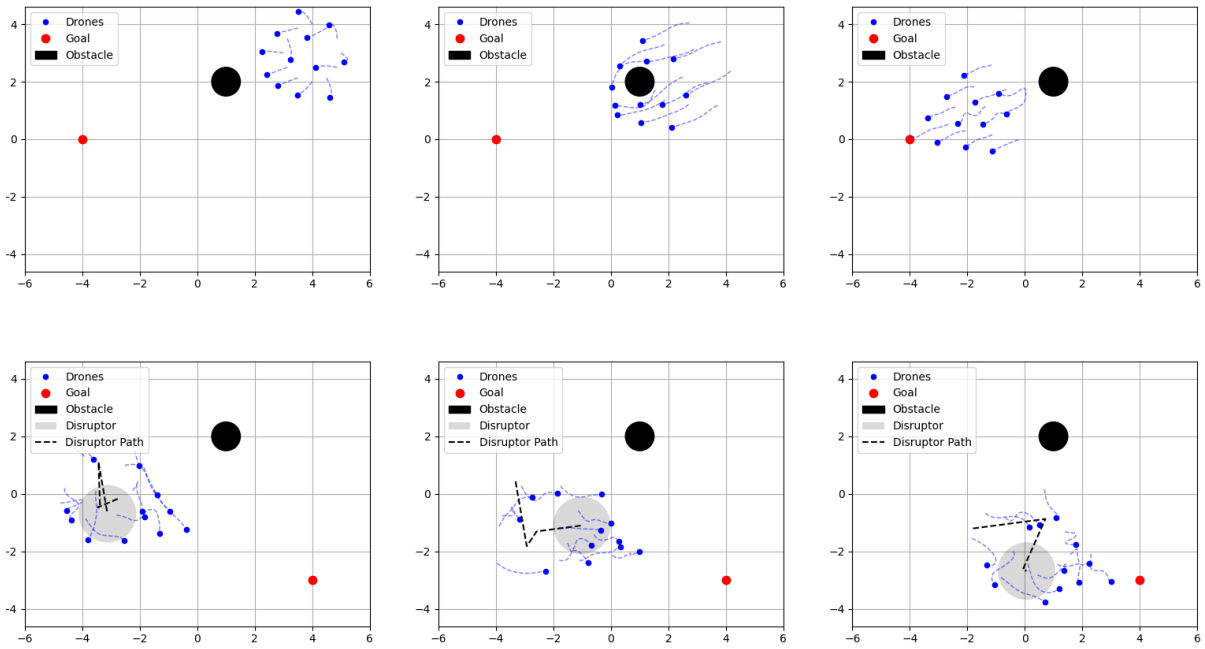

Fig. 5. Graph of the test scenario. The first row shows the formation control and obstacle avoidance. Second row shows the effect of the disruptor (pictured in light gray) on the swarm. While the (arrow-shaped) formation is clearly visible before the disruptor is introduced in the control scheme (top row), the formation is much more difficult to distinguish when it is active (bottom row). In both cases, the formation aims to reach the assigned goal (in red) while avoiding the obstacle (in black).

$[\sigma_v(t), \sigma_\Omega(t)]$ *is the estimated standard error of the linear least-squares problem*

$$\min_{[\mathbf{v}^s, \mathbf{\Omega}]} ||\mathbf{v}(t) - A(t) \begin{bmatrix} \mathbf{v}^s \\ \mathbf{\Omega} \end{bmatrix}||$$

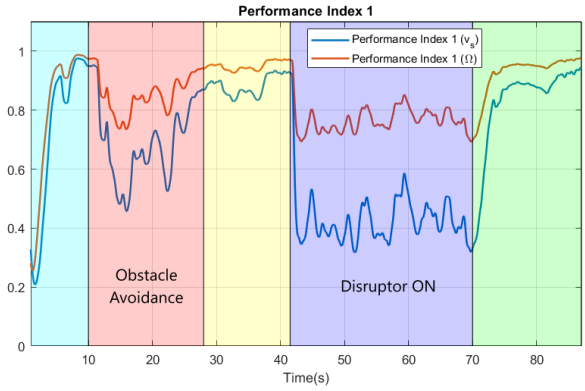

Fig. 6. Amorphousness measured by Performance index 1 (two parameters) in the case of a simulation with obstacle avoidance and a disruptor being activated on a limited time period. The figure shows $f(\sigma_v)$ and $f(\sigma_\Omega)$, with $f(x) = 2 - \frac{2}{1+30e^{-x}}$ for better visualization of the performance index.

Fig. 6 reports the variations of this first metric during a scenario similar to the one described in Section IV-B, but with the distance between the objects (goals, obstacles) being increased to help distinguish the successive steps of the scenario. The stress and torsional flexibility indices are higher during the obstacle avoidance and the active disruptor phases, whereas both indices remain under 0.01 in normal formation flight, which means that it is indeed harder to fit a strict rigid structure on the swarm during these periods. During these two phases, the uncertainty on $\mathbf{\Omega}$ is quite similar for both, while the uncertainty on $\mathbf{v}^s$ is higher during the disruptor active phase.

The second metric is a measure of correlation in velocities between neighbors of the swarm [30] (birds flock in the cited reference). Let $C_n(t)$ be the correlation in velocity of the UAV at a topological distance[5] n:

$$C_n(t) = \frac{1}{N} \sum_{i,j} \langle \mathbf{s}_i(t) \ , \ \mathbf{s}_j(t) \rangle \delta_n^{k_{ij}}$$

In the above, $\mathbf{v}_i$ is the velocity of the UAV i, k_{ij} is the *topological distance* between UAV i and j, δ_b^a is the Kronecker delta function, and

$$\mathbf{s}_i = \frac{\mathbf{v}_i}{\|\mathbf{v}_i\|} - \frac{1}{N} \sum_k \frac{\mathbf{v}_k}{\|\mathbf{v}_k\|}$$

Performance index 2 (Connected correlation, from [30])**.** *This metric is the velocity correlation between the 3 closest neighbors in the sense of the positions* $\mathbf{q} = (\mathbf{q}_1^T, ..., \mathbf{q}_N^T)^T$, *so* $\frac{1}{3}(C_1(t) + C_2(t) + C_3(t))$.

Fig. 7 reports the value of this correlation metric during the same demonstration scenario used for Fig. 6. As with the first metric, we observe a slight degradation while avoiding an obstacle, and a severe degradation when the disruptor is active, showing once again the relevance of our proposed method.

[5]This distance quantifies the structural difference between two graphs in a metric space.

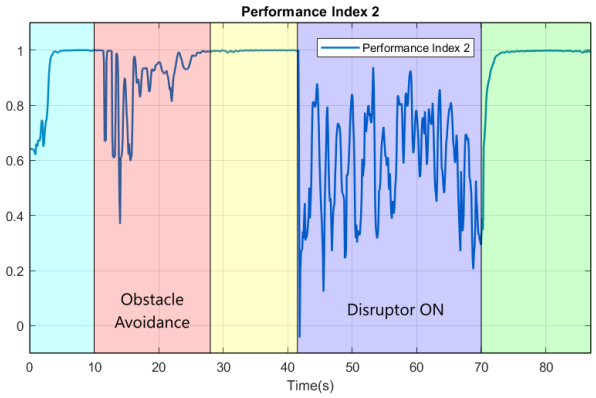

Fig. 7. Amorphousness measured by Performance index 2, in the case of a simulation with obstacle avoidance and a disruptor being activated on a limited time period.

CONCLUSION

In this paper, we addressed the problem of making a swarm structure difficult to detect by using the concept of amorphousness found in the field of material science and condensed physics and adapting it to the case of swarms of UAVs. The method employs a bouncing virtual obstacle meant to disturb the UAV formation by forcing movement inside it. According to the metrics we introduced in Section IV-C this method has promising performance and is straightforward to implement.

The method and its application have been considered in a 2D workspace for the sake of simplicity, but can be generalized easily to the 3D case, as the control method already works well in 3D (see [18]), and the method for amorphousness will only require for the disruptor to move within a sphere rather than a disk. The performance indexes will also be adapted without difficulty. Further studies will also consider experimental validation on the ISL's indoor Crazyflie-based swarm arena.

REFERENCES

[1] A. Kahn, J. Marzat, and H. Piet-Lahanier, "Formation flying control via elliptical virtual structure," in *2013 10th IEEE International Conference on Networking, Sensing and Control (ICNSC)*, pp. 158–163, 2013.

[2] K. Do, "Formation control of mobile agents using local potential functions," in *2006 American Control Conference*, pp. 6 pp.–, 2006.

[3] A. Jadbabaie, J. Lin, and A. Morse, "Coordination of Groups of Mobile Autonomous Agents Using Nearest Neighbor Rules," *Automatic Control, IEEE Transactions on*, vol. 48, pp. 988 – 1001, July 2003.

[4] S. Adinandra, E. Schreurs, and H. Nijmeijer, "A Practical Model Predictive Control for A Group of Unicycle Mobile Robots," *IFAC Proceedings Volumes*, vol. 45, no. 17, pp. 472–477, 2012.

[5] R. Van Parys and G. Pipeleers, "Distributed MPC for multi-vehicle systems moving in formation," *Robotics and Autonomous Systems*, vol. 97, pp. 144–152, 2017.

[6] H. Do, H. Hua, M. Nguyen, V. Nguyen, H. Nguyen, and N. Nga, "Formation Control Algorithms for Multiple-UAVs: A Comprehensive Survey," *EAI end Tr. on Industrial Networks and Intelligent Systems*, vol. 8, pp. 1–13, June 2021.

[7] M. A. Kamel, X. Yu, and Y. Zhang, "Formation control and coordination of multiple unmanned ground vehicles in normal and faulty situations: A review," *Annual Reviews in Control*, vol. 49, pp. 128–144, 2020.

[8] D. Anh, H. La, T. Nguyen, and J. Horn, "Formation control for autonomous robots with collision and obstacle avoidance using a rotational and repulsive force–based approach," *Int. Journal of Advanced Robotic Systems*, vol. 16, pp. 1–16, May 2019.

[9] D. E. Chang and J. E. Marsden, "Gyroscopic Forces and Collision Avoidance with Convex Obstacles," in *New Trends in Nonlinear Dynamics and Control and their Applications* (W. Kang, C. Borges, and M. Xiao, eds.), pp. 145–159, Springer Berlin Heidelberg, 2003.

[10] S. S. Ge and Y. J. Cui, "New potential functions for mobile robot path planning," *IEEE Transactions on Robotics and Automation*, vol. 16, no. 5, pp. 615–620, 2000.

[11] A. Bernardini, F. Mangiatordi, E. Pallotti, and L. Capodiferro, "Drone detection by acoustic signature identification," *Electronic imaging*, vol. 29, pp. 60–64, 2017.

[12] B. Taha and A. Shoufan, "Machine learning-based drone detection and classification: State-of-the-art in research," *IEEE access*, vol. 7, pp. 138669–138682, 2019.

[13] H. Rahman, M. A. S. Sejan, A. Aziz, R. Tabassum, J.-I. Baik, and H.-K. Song, "A comprehensive survey of unmanned aerial vehicles detection and classification using machine learning approach: Challenges, solutions, and future directions," *Remote Sensing*, vol. 16, no. 5, p. 879, 2024.

[14] Y. Zheng, Z. Chen, D. Lv, Z. Li, Z. Lan, and S. Zhao, "Air-to-air visual detection of micro-UAVs: An experimental evaluation of deep learning," *IEEE Robotics and Automation Lett.*, vol. 6, no. 2, pp. 1020–1027, 2021.

[15] M. Tanzi, S. Farè, and G. Candiani, "Organization, structure, and properties of materials," in *Foundations of Biomaterials Engineering*, pp. 3–103, Academic Press, 2019.

[16] Z.-Q. Hu, A.-M. Wang, and H.-F. Zhang, "Amorphous materials," in *Modern Inorganic Synthetic Chemistry (Second Edition)* (R. Xu and Y. Xu, eds.), pp. 641–667, Amsterdam: Elsevier, second ed., 2017.

[17] A. Guinier, *X-ray diffraction: in crystals, imperfect crystals, and amorphous bodies*. Courier Corporation, 2013.

[18] B. Piet, M. Ablak, G. Strub, S. Changey, and N. Petit, "Experiments of high-level formation flight of a medium scaled swarm of micro UAV in a confined environment with obstacle," in *Proc. of 2025 AIAA SciTech (to appear)*, 2025.

[19] J. P. Crutchfield, "Between order and chaos," *Nature Physics*, vol. 8, no. 1, pp. 17–24, 2012.

[20] M. Li, P. Vitányi, *et al.*, *An introduction to Kolmogorov complexity and its applications*, vol. 3. Springer, 2008.

[21] A. N. Sayed, O. M. Ramahi, and G. Shaker, "Frequency-modulated continuous-wave radar perspectives on unmanned aerial vehicle detection and classification: A primer for researchers with comprehensive machine learning review and emphasis on full-wave electromagnetic computer-aided design tools," *Drones*, vol. 8, no. 8, p. 370, 2024.

[22] V. P. Riabukha, "Radar surveillance of unmanned aerial vehicles," *Radioelectronics and Communications Systems*, vol. 63, no. 11, pp. 561–573, 2020.

[23] Y. Waseda, E. Matsubara, and K. Shinoda, *X-ray diffraction crystallography: introduction, examples and solved problems*. Springer Science & Business Media, 2011.

[24] F. Hoffmann, M. Ritchie, F. Fioranelli, A. Charlish, and H. Griffiths, "Micro-doppler based detection and tracking of UAVs with multistatic radar," in *2016 IEEE radar conference (RadarConf)*, pp. 1–6, 2016.

[25] J. Ren and X. Jiang, "A three-step classification framework to handle complex data distribution for radar UAV detection," *Pattern Recognition*, vol. 111, pp. 1–11, 2021.

[26] A. Martian, F. Chiper, R. Craciunescu, C. Vladeanu, O. Fratu, and I. Marghescu, "RF based UAV detection and defense systems: Survey and a novel solution," in *2021 IEEE int. Black Sea conf. on communications and networking (BlackSeaCom)*, pp. 1–4, IEEE, 2021.

[27] A. Rosu-Finsen, M. B. Davies, A. Amon, H. Wu, A. Sella, A. Michaelides, and C. G. Salzmann, "Medium-density amorphous ice," *Science*, vol. 379, no. 6631, pp. 474–478, 2023.

[28] B. Brogliato and A. Tanwani, "Dynamical systems coupled with monotone set-valued operators: Formalisms, applications, well-posedness, and stability," *Siam Review*, vol. 62, no. 1, pp. 3–129, 2020.

[29] P. Billingsley, *Probability and Measure*. Wiley Series in Probability and Statistics, Wiley, 1995.

[30] A. Cavagna, L. Del Castello, S. Dey, I. Giardina, S. Melillo, L. Parisi, and M. Viale, "Short-range interactions versus long-range correlations in bird flocks," *Phys. Rev. E*, vol. 92, pp. 1–21, Jul 2015.